Article

The Control of Isolated Kerogen on Pore Structure and Heterogeneity in Marine-Continental Transitional Shale: A Case Study on the Taiyuan Formation, Northern Ordos Basin

Zhengxi Gao [1], Ke Miao [2,*], Yushan Zuo [1], Fuhua Shang [3,4], Shuang Gao [2], Wentian Mi [2], Yuan Gao [2], Qing Li [1] and Haidong Li [5]

[1] Inner Mongolia Key Laboratory of Magmatic Mineralization and Ore-Prospecting, Hohhot 010020, China
[2] College of Resource and Environmental Engineering, Inner Mongolia University of Technology, Hohhot 010051, China
[3] Shaanxi Key Laboratory of Petroleum Accumulation Geology, Xi'an 710065, China
[4] Inner Mongolia Engineering Research Center of Geological Technology and Geotechnical Engineering, Inner Mongolia University of Technology, Hohhot 010051, China
[5] Inner Mongolia Mining Development Limited Liability Company, Hohhot 010020, China
* Correspondence: miaoke6453@163.com; Tel.: +86-17331006453

Abstract: Accurately determining the pore structure and heterogeneity characteristics of marine-continental transitional shale in the Taiyuan Formation is crucial for evaluating the shale gas resources in the northern Ordos Basin. However, the studies on pore characteristics and heterogeneity of marine-continental transitional shales and isolated kerogen are limited. This study collected Taiyuan Formation shale in the northern Ordos Basin, and corresponding kerogen isolated from shale and used N_2 and CO_2 adsorption experiment and Frenkel–Halsey–Hill and Volume-Specific Surface Area model to investigate the pore structure and heterogeneity of both. The results show that the isolated kerogen is dominated by micropores, and the micropore's specific surface area and volume are 4.7 and 3.5 times the corresponding shale, respectively. In addition, the microporous heterogeneity of the isolated kerogen is stronger than that of shale, while the mesoporous heterogeneity is exactly the opposite. Meanwhile, the micropores fractal dimension D_m is positively correlated with organic matter (OM) content, while mesopores fractal dimension D_1 and D_2 are negatively linearly correlated with TOC content and have no significant relationship with clay mineral and quartz content (but show a significant positive correlation with illite and illite/smectite mixed layer). Isolated kerogen plays an important role in the pore (especially micropores) heterogeneity of shale, while other minerals (such as clay minerals) have a controlling effect on the mesopores heterogeneity of shale. Compared with marine shale, the marine-continental transitional shale of the Taiyuan Formation has a lower fractal dimension and better connectivity, which is conducive to shale gas seepage and migration. The final result can provide a significant basis for the reserve evaluation and the optimization of desert areas in the marine-continental transitional shale gas in the northern Ordos Basin.

Keywords: Ordos Basin; marine-continental transitional shale; isolated kerogen; fractal dimension; shale gas reserves

1. Introduction

In 2023, the shale gas production of Longmaxi marine shales in the Sichuan Basin reached 250×10^8 m³ and became a crucial part of the natural gas supply [1,2]. Hence, oil and gas experts in China have mainly focused on Longmaxi marine shales in the Sichuan Basin, and pore structure characteristics have been extensively studied [3–5]. In fact, marine-continental transitional shales have also been proven to have good shale gas resource potential [6–8]. However, compared to the Longmaxi marine shale, the research on pore structure and heterogeneity of marine-continental transitional shale is still relatively weak due to its variable sedimentary environment and complex material composition [9,10].

Mandelbrot et al. originally proposed fractal theory to describe the irregularity of complex structures and applied it to geology research [11,12]. Subsequently, Katz and Thompson applied fractal theory to the study of shale pores heterogeneity and proved that shale pores have obvious fractal characteristics, and the fractal dimension can well represent the shape complexity and spatial distribution heterogeneity of pores [13]. At present, scholars usually use image analysis (for example, field emission scanning electron microscopy, nuclear magnetic resonance technology) and fluid injection (such as mercury injection method gas adsorption experiment) to characterize the pore structure of shale and use fractal theory to quantitatively describe the complexity and heterogeneity of pore structure [14–17]. Li et al. used NMR and FE-SEM to investigate the pore characteristics and fractal dimension of marine shales and discovered that shales with larger surface fractal dimensions have higher methane adsorption capacity, while volume fractal dimension has no significant effect on methane adsorption capacity [18]. Sun et al. studied shale fractal characteristics by NMR and considered that recrystallization during diagenesis decreases the complexity of seepage flow pores [19]. Li et al. used the Frenkel–Halsey–Hill (FHH) model based on the N_2 adsorption experiment and observed shale pore has obvious fractal characteristics and believed that shale pore structure heterogeneity is more complex than shale surface heterogeneity [20]. Tian et al. combined the previous methods to explore the fractal dimension of shale with different maturity and discovered that with the improvement of maturity, the surface fractal dimension of shale changes to the mass fractal dimension [21].

Previous studies have suggested that kerogen has an undeniable impact on the complexity and heterogeneity of shale reservoirs, including content, type, and maturity [15,20–22]. Peng et al. calculated the Longmaxi shale fractal dimension by the FHH fractal model and discovered that it has a significantly positive linear relation with TOC content [23]. However, some other scholars believe that the content of OM has little effect on the heterogeneity of pores [24]. Currently, the influence of OM on shale pore heterogeneity is still controversial. In addition, Chang et al. calculated and compared the fractal dimension of continental and marine shales by using N_2 adsorption and FHH models, respectively, and proposed that OM has a more obvious influence on the pore structure and fractal dimension of marine shales [22]. However, compared with marine and continental shales, marine-continental transitional shales have more abundant OM sources and more variable sedimentary environments, which have more complex pore structures and stronger heterogeneity [25,26]. Therefore, the heterogeneity of marine-continental transitional shale kerogen and its contribution to shale heterogeneity need to be further studied.

In this paper, a low-pressure CO_2/N_2 adsorption experiment was applied to characterize the shale and corresponding isolated kerogen pore structure, and Volume-Specific Surface Area (V-S) and FHH models were utilized to calculate the pore fractal dimension. Meanwhile, the control of kerogen on the pore structure and heterogeneity of shale was explored. This is crucial for the exploration and extraction of northern Ordos Basin shale gas.

2. Materials and Methods

2.1. Geological Setting and Sample Preparation

Ordos Basin, a major oil and gas basin of China, is a large inland basin developed on the basis of the North China Platform [27,28]. The regional tectonics of the Ordos Basin are divided into six secondary tectonic units: Tianhuan depression, Yimeng uplift, Western thrust belt, Jinxi flexural fold belt, Yishan slope, and Weibei uplift (Figure 1a) [29–31]. The Taiyuan Formation of the Carboniferous system is almost distributed at the whole basin and is a marine-continental transitional facies deposit. The lithology comprises grayish-white sandstone, siltstone, coal, grayish-black mudstone, and carbonaceous mudstone, and the organic-rich shale is also well-developed (Figure 1b) [32–34].
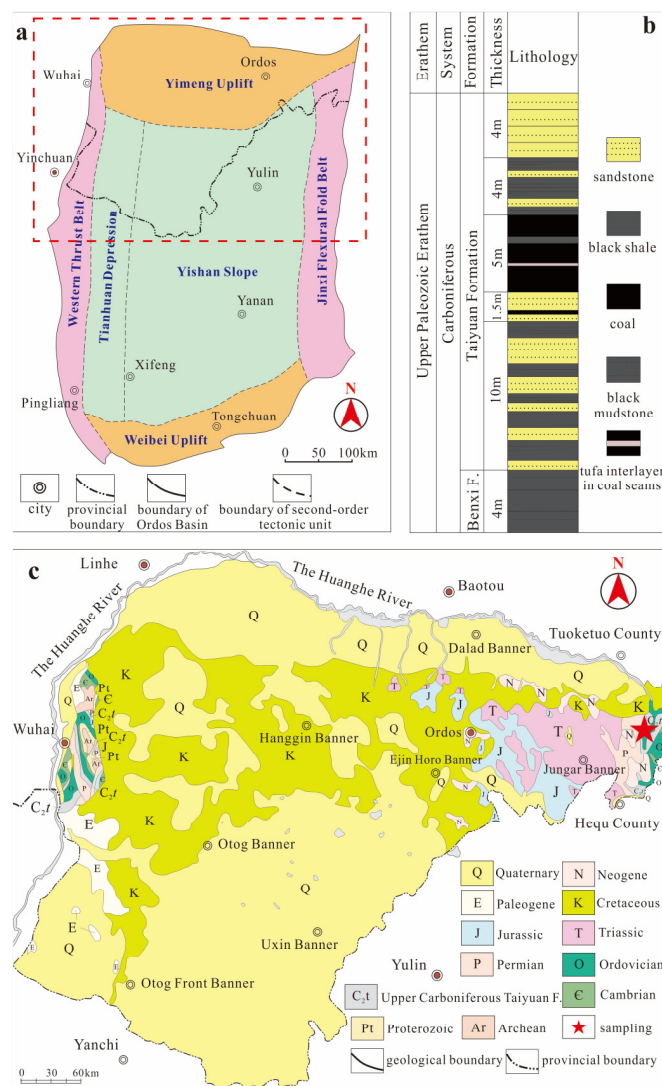
Figure 1. (**a**) Tectonic map of Ordos Basin and study area (modified by Cao et al., 2024) [28]. (**b**) Sedimentary sequence at the sampling site. (**c**) Geological map of northern Ordos Basin (modified from Yang et al., 2018) [32].

The research area is located in the northern Ordos Basin, where the earth's surface is largely covered by the Quaternary and Cretaceous systems, with the Taiyuan Formation only emerging in the Junge Banner and Wuhai areas on the edge of the basin (Figure 1c). We took seven samples from the Taiyuan Formation shales of Junge Banner, which is a series of delta-dominated marine-continental transitional deposits.

2.2. Experimental Methods

2.2.1. Organic Geochemical and Mineralogical Analyses

The shale sample is crushed to 80–200 mesh before TOC content determination, with sufficient 10% hydrochloric acid solution to completely remove carbonate from the sample. All steps refer to "Determination for total organic carbon in sedimentary rock" (GB/T 19145-2022) [35].

The mineralogical composition of the shales was determined through the XRD analyses. Before the determination, shale samples are crushed to 40 mesh, grinding without granular feeling, and scanning speed: 2θ is 2°/min; 2θ scanning range: 5°~45°; sampling step width: 2θ is 0.02°; test procedure refers to SY/T 5163-2018 [36].

The method and process of extracting kerogen from shale samples are referred to the national standard of the People's Republic of China (GB/T 19144-2010) [37], and kerogen sample numbers were YG-1K, YG-2K, YG-3K, YG-4K, YG-5K, YG-6K, YG-7K.

2.2.2. Gas Adsorption Experiment

N_2 and CO_2 adsorption tests were conducted on shale samples and kerogen samples. The shales were ground to 60 mesh and placed in a vacuum for 20 h before the experiment. The experimental temperature is -196 °C (77 K), and the N_2 adsorption equilibrium pressure (P/P_0) is between 0.001 to 0.995. The CO_2 adsorption experiment temperature is 0 °C (273.5 K), and the (P/P_0) is 0.0001–0.032. The pore characteristics were measured by adopting the Barrett–Johner–Halenda (BJH) model and Brunauer–Emmett–Teller (BET) model. Pore SSA and pore volume of micropores (0–2 nm) were measured through a density functional theory (DFT) model [38,39].

2.2.3. Fractal Calculation

The fractal theory of quantitative evaluation is described by the fractal dimension D. Depending on gas adsorption-desorption theory, the FHH model has been extensively applied to calculate the porous media fractal feature [40–42]. The fractal dimension is calculated by the Equation (1):

$$\mathrm{Ln}V = A\mathrm{Ln}(\mathrm{Ln}(P_0/P)) + \text{constant} \tag{1}$$

$$D = A + 3 \tag{2}$$

where: V is the cumulative volume at the balance pressure P. A is the slope of the curve for $\mathrm{Ln}(\mathrm{Ln}(P_0/P))$, and $\mathrm{Ln}V$. P_0 is saturation pressure; The fractal dimension is obtained by Equation (2). Based on the gas adsorption and FHH model, two asymptotes were able to draw at P/P_0 in the 0–0.45 and 0.45–1.0 range. The fractal dimension D_1 corresponds to the P/P_0 range of 0–0.45; it is monolayer absorption and is primarily controlled by the Van der Waals force. The fractal dimension D_2 is obtained from N_2 adsorption data in P/P_0 between 0.45 and 1, which is multilayer adsorption and affected by capillary coagulation [43,44].

The Volume-Specific Surface Area (V-S) model was proposed by Mandelbrot et al. and calculated the corresponding pore fractal dimension by using the correlation between pore volume and the SSA of solid porous media [12]. At present, it has been shown that it is highly applicable to the research of shale micropore structure characteristics [45]. The calculation process is as follows:

$$\mathrm{Ln}V = \frac{3}{D_\mathrm{m}}\mathrm{Ln}S + \text{constant} \tag{3}$$

where: V is cumulative pore volume, cm^3/g; D_m is micropores fractal dimension; S is cumulative SSA, m^2/g.

3. Results

3.1. Mineral Composition and Organic Geochemical Characteristics

Table 1 shows the organic geochemistry and mineral component of the Taiyuan Formation shale in the northern Ordos Basin. The shale samples have low quartz content and high clay content, and TOC content ranges from 1.06–7.5%, with an average of 2.89%. OM content exceeds the requirement of the target section of the marine-continental transitional shale gas field. The main mineral component is clay minerals, mainly kaolinite.

Table 1. Organic geochemical and mineralogical parameters of samples.

Sample	TOC (%)	Quartz (%)	Potash Feldspar (%)	Clay Minerals (%)	Illite (%)	Kaolinite (%)	Chlorite (%)	I/S Mixed Layer (%)
YG-1	1.40	20.7	0.0	79.3	7	81	6	6
YG-2	1.30	37.8	0.9	61.3	9	75	7	9
YG-3	1.28	15.8	0.0	84.2	5	82	6	7
YG-4	1.06	19.2	0.0	80.8	6	79	8	7
YG-5	1.38	20.5	0.0	79.5	9	80	6	5
YG-6	6.34	4.7	0.0	95.3	4	86	8	2
YG-7	7.50	34.1	0.0	65.9	5	84	9	2

3.2. Gas Adsorption Characteristics

Table 2 illustrates the pore characteristics of Taiyuan shale and kerogen in the northern Ordos Basin. The micropore, mesopores, and macropores SSA of shale range from 8.15–21.01 m^2/g (average value is 12.68 m^2/g), 14.46–17.90 m^2/g (mean is 16.26 m^2/g) and 0.1502–0.3255 m^2/g (average value is 0.2101 m^2/g), respectively. The micropore, mesopores, and macropores volume of shale range from 0.003225–0.006998 cm^3/g (average 0.004774 cm^3/g), 0.02794–0.04054 cm^3/g (average 0.03404 cm^3/g) and 0.002979–0.006462 cm^3/g (average 0.004158 cm^3/g), respectively.

Table 2. Pore structure parameters of samples.

Sample	Micropore (<2 nm) Specific Surface Area (m²/g)	Micropore (<2 nm) Volume (cm³/g)	Mesoporous (2–50 nm) Specific Surface Area (m²/g)	Mesoporous (2–50 nm) Volume (cm³/g)	Macropore (>50 nm) Specific Surface Area (m²/g)	Macropore (>50 nm) Volume (cm³/g)
YG-1	11.16	0.004609	17.90	0.03860	0.2283	0.004421
YG-2	10.60	0.004327	14.46	0.03050	0.1685	0.003384
YG-3	8.150	0.003225	15.60	0.02794	0.1502	0.002979
YG-4	9.015	0.003696	16.15	0.02876	0.1565	0.003073
YG-5	9.977	0.004436	17.69	0.03233	0.1631	0.003229
YG-6	21.01	0.006998	15.66	0.04054	0.2788	0.005559
YG-7	18.87	0.006127	16.36	0.03963	0.3255	0.006462
YG-1K	74.85	0.02107	4.234	0.01435	0.2371	0.005425
YG-2K	51.51	0.01463	3.676	0.00859	0.1364	0.002700
YG-3K	36.95	0.01065	2.653	0.00734	0.1398	0.002800
YG-4K	41.64	0.01282	2.320	0.00696	0.1624	0.003293
YG-5K	56.53	0.01626	3.562	0.00993	0.2017	0.003857
YG-6K	55.06	0.01607	3.076	0.00886	0.1575	0.003032
YG-7K	74.43	0.02140	1.595	0.00494	0.1007	0.002103

The micropore, mesopores, and macropores SSA of shale kerogen range from 36.95–74.85 m^2/g (average value is 55.85 m^2/g), 1.595–4.234 m^2/g (average value is 3.017 m^2/g) and 0.1007–0.2371 m^2/g m^2/g (average value is 0.1622 m^2/g), respectively. The micropore, mesopores, and macropores volume of shale kerogen range from 0.01065–0.02140 cm^3/g (average 0.01613 cm^3/g), 0.00494–0.01435 cm^3/g (average value is 0.008708 cm^3/g) and 0.002103–0.005425 cm^3/g (average 0.003316 cm^3/g), respectively.

3.3. Results of Fractal Dimension Calculation

3.3.1. Mesoporous Fractal Parameter of Shale and Kerogen

Figures 2 and 3 show mesoporous fractal dimension analysis of shale and kerogen. Table 3 shows the fractal dimension result of Taiyuan Formation shale and kerogen in the northern Ordos Basin. The shale fractal dimension D_1 and D_2, respectively, ranges from 2.317–2.433 and 2.585–2.701. The shale fractal dimension D_1 and D_2, respectively, ranges

from 2.317–2.433 and 2.585–2.701. The kerogen fractal dimension D_1 is between 2.19–2.38, and D_2 is between 2.51–2.58.
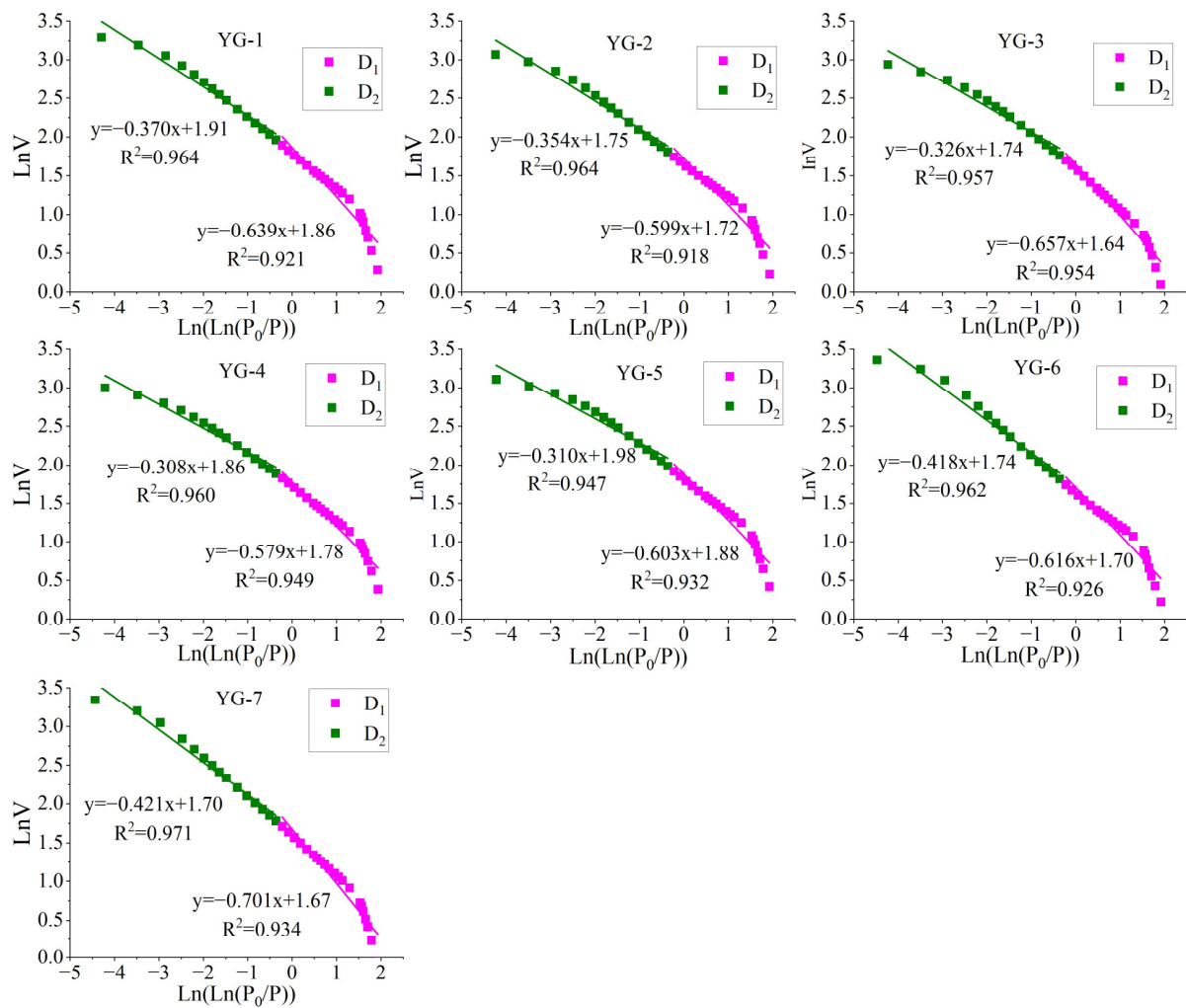
Figure 2. Fractal dimension fitting of shale mesoporous.

Table 3. Mesoporous fractal dimension of Taiyuan Formation shale and kerogen in northern Ordos Basin.

Sample	P/P0 = 0~0.45		P/P0 = 0.45~1	
	D_1	R^2	D_2	R^2
YG-1	2.36	0.921	2.63	0.964
YG-2	2.40	0.918	2.65	0.964
YG-3	2.34	0.954	2.67	0.957
YG-4	2.42	0.949	2.69	0.96
YG-5	2.40	0.932	2.69	0.947
YG-6	2.38	0.926	2.58	0.962
YG-7	2.30	0.934	2.58	0.971
YG-1K	2.36	0.944	2.51	0.994
YG-2K	2.35	0.965	2.58	0.999
YG-3K	2.36	0.949	2.55	0.999
YG-4K	2.30	0.94	2.51	0.995
YG-5K	2.38	0.949	2.54	0.998
YG-6K	2.29	0.932	2.52	0.994
YG-7K	2.19	0.908	2.52	0.992
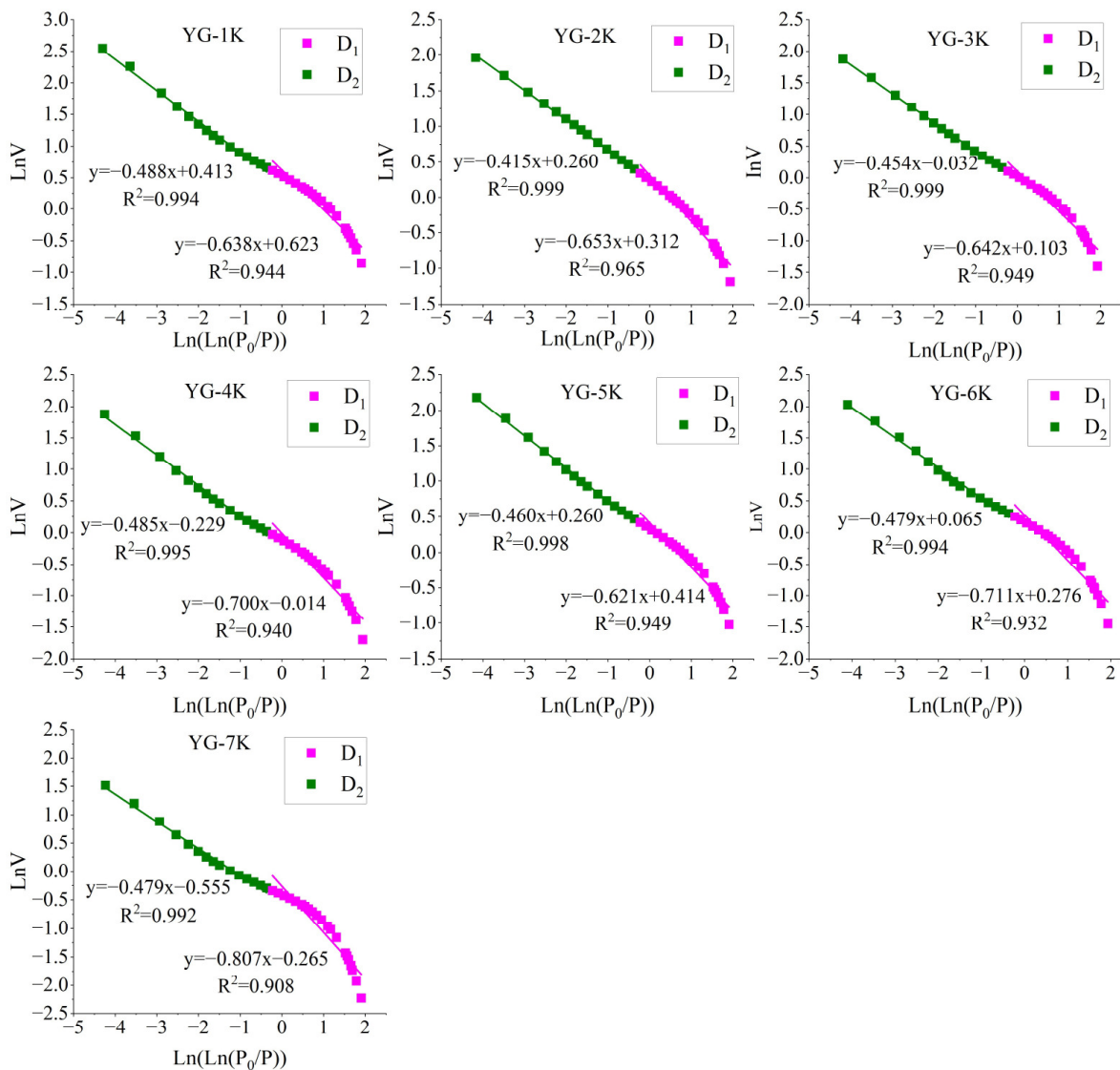
Figure 3. Fractal dimension fitting of kerogen mesoporous.

3.3.2. Micropore Fractal Parameter of Shale and Kerogen

Figures 4 and 5 show the micropore fractal dimension analysis of shale and kerogen mesopore. Table 4 indicates the shale and kerogen fractal dimension result of the Taiyuan Formation. The micropore fractal dimension D_m of shale and kerogen ranges from 2.58–2.71 and 2.67–2.79, with an average of 2.64 and 2.74, respectively.

Table 4. Micropore fractal dimension of Taiyuan Formation shale and kerogen in northern Ordos Basin.

Sample	D_m	R^2	Sample	D_m	R^2
YG-1	2.66	0.999	YG-1K	2.67	0.999
YG-2	2.63	0.999	YG-2K	2.69	0.999
YG-3	2.58	0.999	YG-3K	2.79	0.999
YG-4	2.60	0.999	YG-4K	2.74	0.997
YG-5	2.71	0.999	YG-5K	2.75	0.999
YG-6	2.68	0.999	YG-6K	2.74	0.999
YG-7	2.64	0.999	YG-7K	2.79	0.999
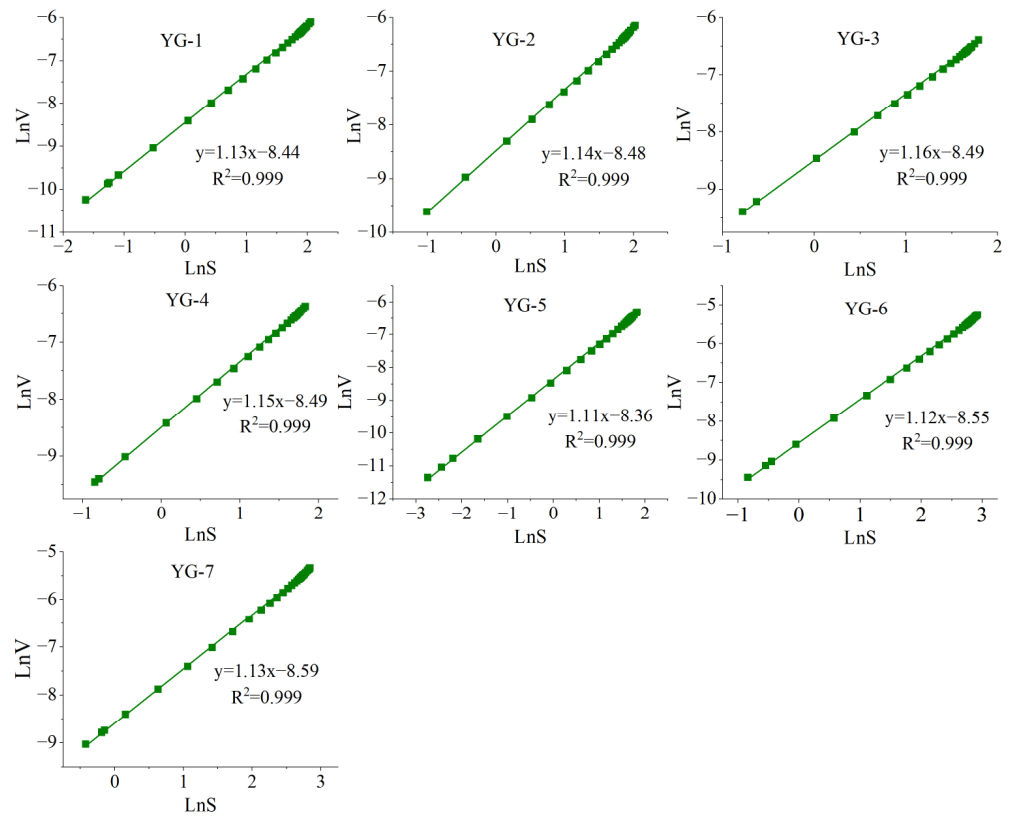
Figure 4. Fractal dimension fitting of shale micropores.
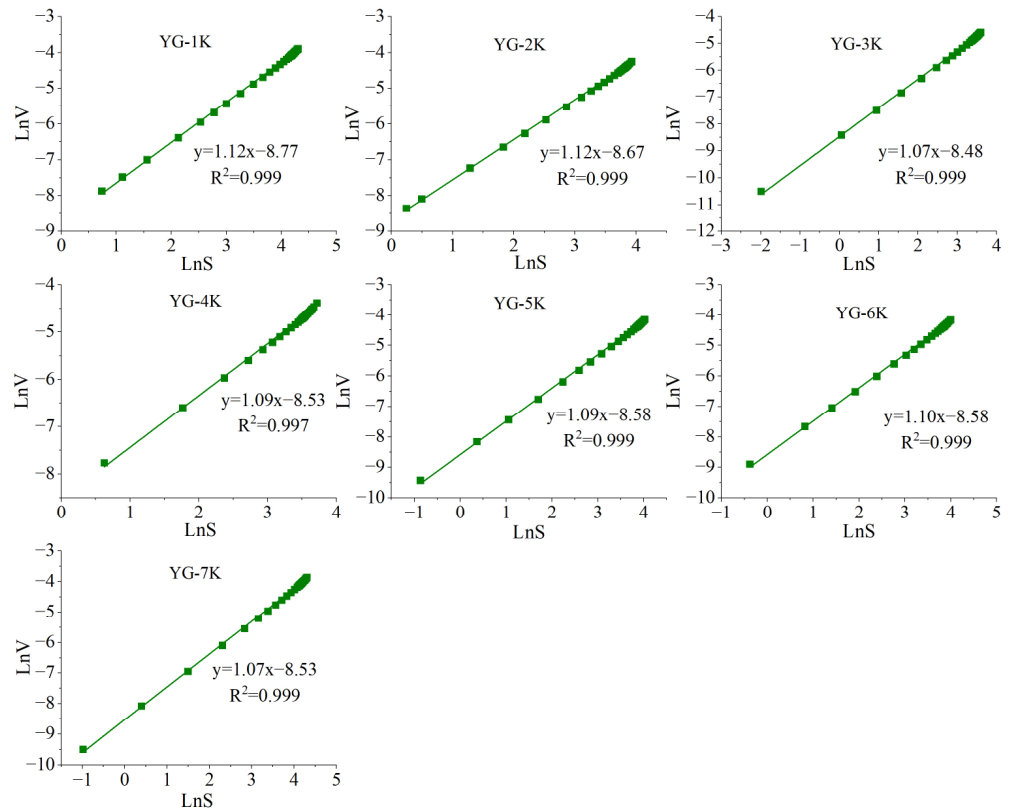
Figure 5. Fractal dimension fitting of kerogen micropores.

4. Discussion

4.1. The Pore Structure and Heterogeneity of Kerogen

Table 2 shows the average pore SSA and pore volume of isolated kerogen samples are 59.03 m^2/g and 28.15 $\times$ 10^{-3} cm^3/g, which are 2 and 0.7 times that of the corresponding shale samples. The micropores SSA and volume of isolated kerogen are 3.7 and 2.5 times higher than that of the corresponding shale, indicating that isolated kerogen has more micropores and significantly contributes to the micropore parameters of the shale. Li et al. also investigated matrix-related pores from differential sedimentary shale and discovered that the pore SSA and volume of isolated kerogen in marine-continental transitional shales were 1 and 0.6 times higher than those of the corresponding shale samples, while the pore SSA and volume of isolated kerogen in marine shale are 8.5 and 3 times higher than the corresponding shale samples [46]. In fact, this difference is attributed to differences in shale kerogen types; marine-continental transitional shale kerogen generally has stronger thermodynamic stability and lower pore contribution ability compared to marine shale, but it still provides a large number of micropores for shale [46–48].

Previous studies have extensively explored the fractal dimension of shale by N$_2$ adsorption experiment and FHH model and used D$_1$ and D$_2$ to characterize the complex features of shale surface and structure, respectively [20,49,50]. In addition, due to the N$_2$ adsorption not characterizing micropores well, some scholars used the CO$_2$ adsorption experiment and V-S model to calculate the micropore's fractal dimension D$_m$ [51–53]. In Figure 6a, we observed that kerogen samples exhibit certain fractal characteristics and heterogeneity, and the heterogeneity of kerogen micropores is much larger than that of kerogen mesopores. Peng et al. have also discovered this phenomenon and pointed out that the complexity of organic pores is influenced by the pore size, and the heterogeneity of organic pores weakens as the pore size increases [23]. Thus, we believe that it is perhaps due to the kerogen developing more micropores and having more complex pore structures in the process of thermal evolution [42,54–56]. In addition, the results of this study have certain similarities with the fractal dimension of shale kerogen in a previous study (Figure 6b) [57]; D$_1$ of the kerogen samples is smaller than D$_2$ and has a positive correlation, indicating that structural heterogeneity of kerogen exceeds that of the surface and increases with the enhancement of shale surface heterogeneity.
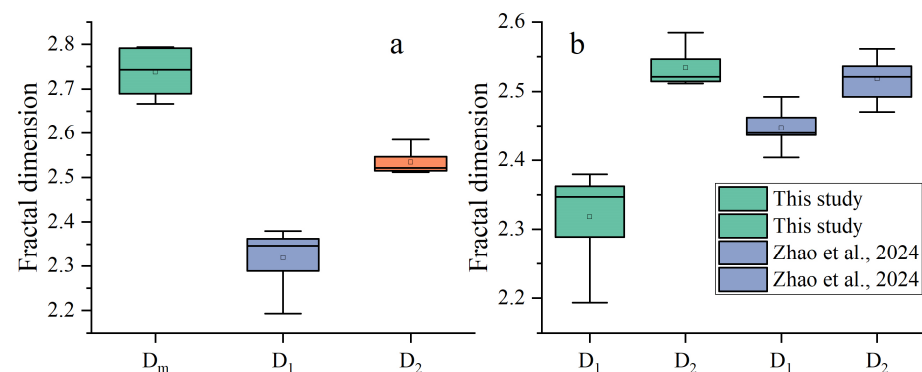
Figure 6. The fractal dimension of marine-continental transitional shale kerogen (**a**) and its comparison with that of marine shale kerogen (**b**) (Zhao et al. 2024) [57].

4.2. Control of Shale Pore Heterogeneity by Kerogen

In Figure 7a, the fractal dimension of Taiyuan shale in the northern Ordos Basin is between 2–3, with obvious fractal characteristics, heterogeneity, and roughness. Shale fractal dimension D$_1$ is smaller than D$_2$, showing that the shale interior structure heterogeneity exceeds the shale surface, while D$_m$ and D$_2$ of shale are close, indicating that the shale micropore and mesoporous heterogeneity are similar. Furthermore, compared with previous studies, the calculated results of this study are basically consistent with the fractal dimensions of marine-continental transitional shale and are smaller than the fractal

dimensions of Marine shale (Figure 7b) [20,46,58–60], suggesting the marine-continental transitional shale has relatively lower heterogeneity and stronger permeability and fluidity. Previous studies believe marine-continental transitional shales tend to have relatively lower OM content and maturity and relatively poorly developed organic pores, which results in a decrease in fractal dimension [22,46].
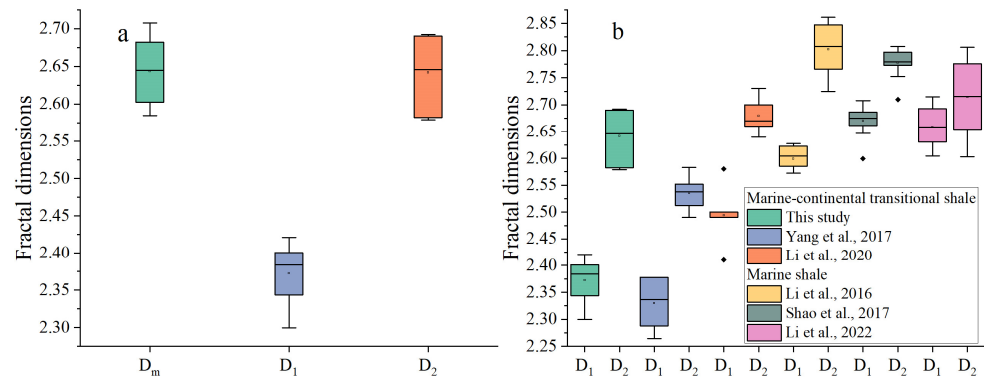
Figure 7. The fractal dimension of Marine-continental transitional shale (**a**) and its comparison with that of Marine shale (**b**) [20,46,58–60].

In this study, the isolated kerogen micropores fractal dimension D_m is greater than shale samples, while the mesoporous fractal dimensions D_1 and D_2 are the opposite (Figure 8). In addition, whether it is shale or isolated kerogen, the microporous fractal dimension D_m is greater than the mesoporous fractal dimension D_1 and D_2 (Figure 8). Thus, we speculate that kerogen can develop more organic pores and microfracture in the thermal evolution process, which are mainly micropores and have complex pore structures and have important contributions to the fractal dimension of shale (Figures 9 and 10) [45,55]. To further elucidate the influence of isolated kerogen on shale heterogeneity, we have drawn the correlation heat map between material composition and pore fractal dimension (Figure 11). TOC content is positively correlated with micropore fractal dimension D_m but negatively correlated with mesoporous fractal dimension D_1 and D_2. In fact, different correlations are determined by the degree of pore development and pore size [18,61,62]. Kerogen develops a large number of micropores, resulting in a gradual increase in the number and heterogeneity of micropores as TOC content increases. Meanwhile, the mesoporous material provided by kerogen is limited, while clay minerals (especially illite and illite/smectite mixed layers) provide more mesopores, resulting in a larger fractal dimension and stronger heterogeneity of shale mesopores (Figure 11).
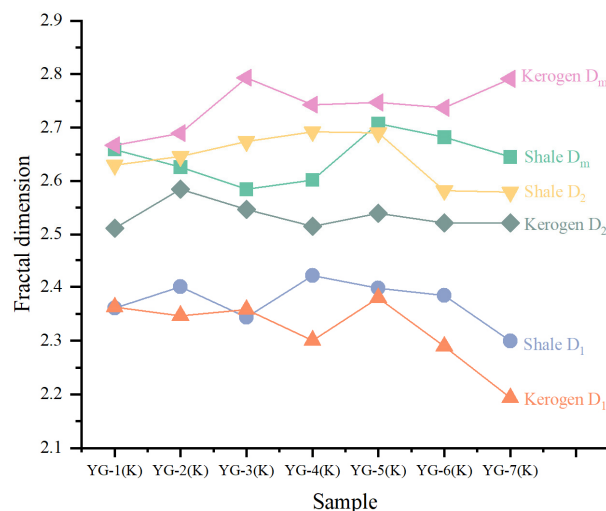
Figure 8. Comparison of different fractal dimensions of shale and kerogen.
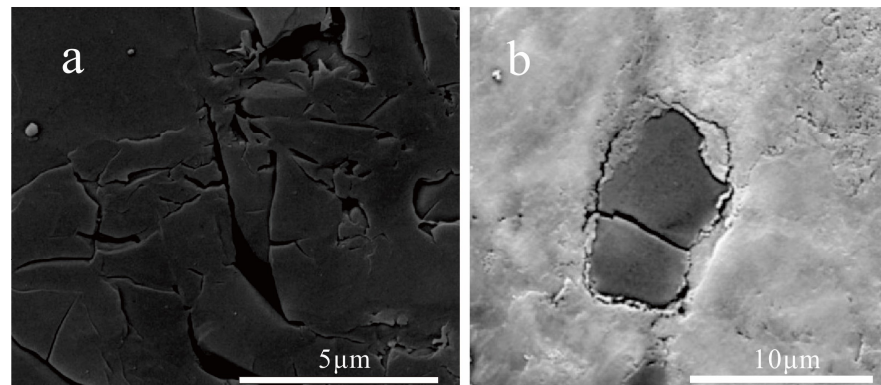
Figure 9. Organic matter hydrocarbon generation pores (**a**) and microcracks (**b**) in Taiyuan Formation shale [32].
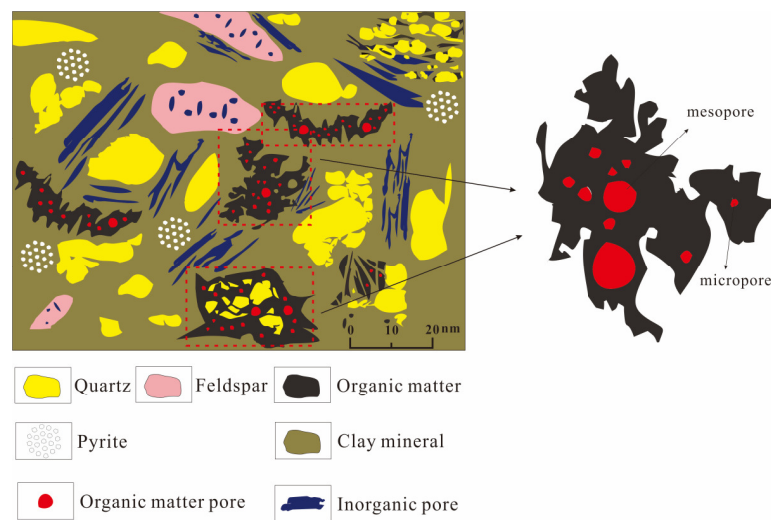
Figure 10. Models of pore fractal characteristics of shale and isolated OM.
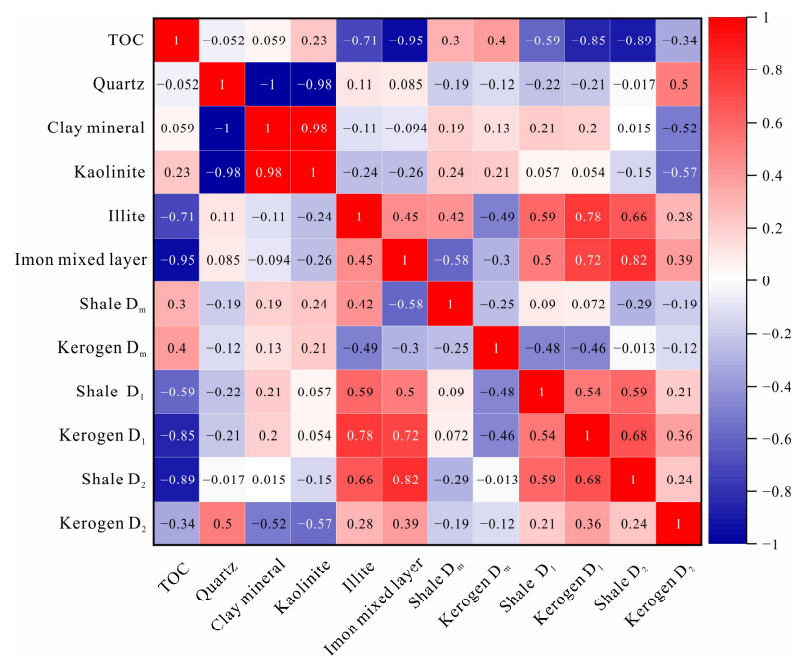
Figure 11. Heat map of correlation between shale material composition and pore parameters.

4.3. Concluding Remarks

The research of shale pores fractal characteristics not only reflects the complexity and diversity of its reservoir space but also has certain geological significance for shale gas evaluation. Previous studies have indicated that the higher fractal dimension shows a more complicated pore structure, which is more conducive to methane adsorption. However, this will also lead to poor permeability of shale reservoirs, resulting in the difficulty of shale gas diffusion and resolution [63,64]. Compared with commercially developed marine shale gas fields, marine-continental transitional shales also have well-developed micropores and mesopores, which can provide abundant shale gas adsorption sites and storage space, which is conducive to the occurrence of adsorbed and free gas. However, the pore heterogeneity of marine-continental transitional shales is lower, suggesting that pores of marine-continental transitional shale have stronger permeability and fluidity, which may lead to shale gas escapes [45,65,66]. Therefore, in the process of exploration in marine-continental transitional shale, high-pressure and closed conditions are significant targets for shale gas fields. Meanwhile, with the continuous maturity of CO_2-enhanced shale gas recovery technology, the advantage of strong permeability of marine-continental transitional shale pores is gradually emerging. Injected CO_2 can more easily enter shale pores, displacing methane and increasing shale gas production [67–69].

5. Conclusions

In this paper, a series of experiments and calculations were carried out, and the pore structure characteristics and fractal features and their influencing factors were investigated. The main conclusions are the following:

(1) The Taiyuan Formation shale in the northern Ordos Basin has low quartz content and high clay content. The shale pores are mainly mesoporous and micropores, and the isolated OM contributes to more micropores.

(2) Based on the FHH and V-S model, the average pore fractal dimensions D_1, D_2, and Dm of isolated kerogen are 2.32, 2.53, and 2.74, respectively. The D_1, D_2, and Dm of shale pores are 2.37, 2.64, and 2.64, respectively. The microporous fractal dimension Dm of isolated kerogen is larger than that of shale, while the mesoporous fractal dimension D_1 and D_2 is exactly the opposite.

(3) The D_m is positively correlated with TOC content, while D_1 and D_2 are exactly the opposite. D_m, D_1, and D_2 have no significant relationship with clay mineral and quartz content (but D_1 and D_2 show a significant positive correlation with illite and illite/smectite mixed layer). Kerogen has a significant contribution to the heterogeneity of micropores, while other minerals have a greater contribution to the mesoporous heterogeneity.

Author Contributions: Z.G. and K.M. wrote the main manuscript text. S.G. completed the experiment and data processing. Other authors contributed to the preparation and revision of the manuscript. All authors have read and agreed to the published version of the manuscript.

Data Availability Statement: The original contributions presented in the study are included in the article; further inquiries can be directed to the corresponding author.

Conflicts of Interest: Author Haidong Li was employed by the Inner Mongolia Mining Development Limited Liability Company. The remaining authors declare that the research was conducted in the absence of any commercial or financial relationships that could be construed as a potential conflict of interest. The Inner Mongolia Mining Development Limited Liability Company had no role in the design of the study; in the collection, analyses, or interpretation of data; in the writing of the manuscript, or in the decision to publish the results.

Abbreviations

TOC	Total Organic Carbon
OM	Organic matter
D_1	mesoporous surface fractal dimension
D_2	mesoporous structure fractal dimensions
D_m	micropores fractal dimensions
FHH	Frenkel–Halsey–Hill
V-S	Volume-Specific Surface Area

References

1. Gao, Y.; Wang, B.; Hu, Y.D.; Gao, Y.J.; Hu, A.L. Development of China's natural gas: Review 2023 and outlook 2024. *Nat. Gas Ind.* **2024**, *44*, 166–177.
2. Zou, C.N.; Lin, M.; Ma, F.; Liu, H.; Yang, Z.; Zhang, G.; Yang, Y.; Guan, C.; Liang, Y.; Wang, Y.; et al. Development, challenges and strategies of natural gas industry under carbon neutral target in China. *Pet. Explor. Dev.* **2024**, *51*, 476–497. [CrossRef]
3. Shang, F.; Zhu, Y.; Hu, Q.; Zhu, Y.; Wang, Y.; Du, M.; Han, Y. Characterization of methane adsorption on shale of a complex tectonic area in Northeast Guizhou, China: Experimental results and geological significance. *J. Nat. Gas Sci. Eng.* **2020**, *84*, 103676. [CrossRef]
4. Wang, Y.; Cheng, H.; Hu, Q.; Liu, L.; Jia, L.; Gao, S.; Wang, Y. Pore structure heterogeneity of Wufeng-Longmaxi shale, Sichuan Basin, China: Evidence from gas physisorption and multifractal geometries. *J. Pet. Sci. Eng.* **2022**, *208*, 109313. [CrossRef]
5. Zheng, Y.; Liao, Y.; Wang, J.; Xiong, Y.; Wang, Y. Factors controlling the heterogeneity of shale pore structure and shale gas production of the Wufeng–Longmaxi shales in the Dingshan plunging anticline of the Sichuan Basin, China. *Int. J. Coal Geol.* **2024**, *282*, 104434. [CrossRef]
6. Wang, E.Z.; Guo, T.; Liu, B.; Li, M.; Xiong, L.; Dong, X.; Zhang, N.; Wang, T. Lithofacies and pore features of marine-continental transitional shale and gas enrichment conditions of favorable lithofacies: A case study of Permian Longtan Formation in the Lintanchang area, southeast of Sichuan Basin, SW China. *Pet. Explor. Dev.* **2022**, *49*, 1310–1322. [CrossRef]
7. He, Q.; Chen, S.; Li, S.; Guo, B.; Lu, J.; Li, Y.; Li, X.; Zhao, L.; Ma, Z. Organic geochemical characteristics and hydrocarbon generation mechanism of marine-continental transitional organic-rich shale: A case study from the Shanxi formation in the eastern margin of the Ordos Basin. *J. Pet. Sci. Eng.* **2022**, *219*, 111116. [CrossRef]
8. Cao, T.; Deng, M.; Xiao, J.; Liu, H.; Pan, A.; Cao, Q. Reservoir characteristics of marine–continental transitional shale and gas-bearing mechanism: Understanding based on comparison with marine shale reservoir. *J. Nat. Gas Geosci.* **2023**, *8*, 169–185. [CrossRef]
9. Xi, Z.; Tang, S.; Wang, J.; Yang, G.; Li, L. Formation and development of pore structure in marine-continental transitional shale from northern China across a maturation gradient: Insights from gas adsorption and mercury intrusion. *Int. J. Coal Geol.* **2018**, *200*, 87–102. [CrossRef]
10. Huang, W.; Ma, X.; Zhou, X.; Liu, J.; He, T.; Tao, H.; Li, S.; Hao, L. Characteristics and controlling factors of pore structure of shale in the 7th member of Yanchang Formation in Huachi area, Ordos Basin, China. *J. Nat. Gas Geosci.* **2023**, *8*, 319–336. [CrossRef]
11. Mandelbrot, B.B. *Les Objets Fractals: Forme, Hasard et Dimension*; Flammarion: Paris, France, 1975.
12. Mandelbrot, B.B.; Passoja, D.E.; Paullay, A.J. Fractal character of fracture surfaces of metals. *Nature* **1984**, *308*, 721–722. [CrossRef]
13. Katz, A.; Thompson, A.H. Fractal sandstone pores: Implications for conductivity and pore formation. *Phys. Rev. Lett.* **1985**, *54*, 1325. [CrossRef] [PubMed]
14. Liu, J.; Lu, D.; Li, P. Nano-scale dual-pore-shape structure and fractal characteristics of transitional facies shale matrix. *J. Nat. Gas Sci. Eng.* **2019**, *68*, 102907. [CrossRef]
15. Ma, B.; Hu, Q.; Yang, S.; Zhang, T.; Qiao, H.; Meng, M.; Zhu, X.; Sun, X. Pore structure typing and fractal characteristics of lacustrine shale from Kongdian Formation in East China. *J. Nat. Gas Sci. Eng.* **2021**, *85*, 103709. [CrossRef]
16. Zhang, J.; Xiao, X.; Wang, J.; Lin, W.; Han, D.; Wang, C.; Li, Y.; Xiong, Y.; Zhang, X. Pore structure and fractal characteristics of coal-bearing Cretaceous Nenjiang shales from Songliao Basin, Northeast China. *J. Nat. Gas Geosci.* **2024**, *9*, 197–208. [CrossRef]
17. Yao, P.; Zhang, J.; Lv, D.; Vandeginste, V.; Chang, X.; Zhang, X.; Wang, D.; Han, S.; Liu, Y. Effect of water occurrence in coal reservoirs on the production capacity of coalbed methane by using NMR simulation technology and production capacity simulation. *Geoenergy Sci. Eng.* **2024**, *243*, 213353. [CrossRef]

18. Li, A.; Ding, W.; Jiu, K.; Wang, Z.; Wang, R.; He, J. Investigation of the pore structures and fractal characteristics of marine shale reservoirs using NMR experiments and image analyses: A case study of the Lower Cambrian Niutitang Formation in northern Guizhou Province, South China. *Mar. Pet. Geol.* **2018**, *89*, 530–540. [CrossRef]

19. Sun, W.; Zuo, Y.; Wu, Z.; Liu, H.; Xi, S.; Shui, Y.; Wang, J.; Liu, R.; Lin, J. Fractal analysis of pores and the pore structure of the Lower Cambrian Niutitang shale in northern Guizhou province: Investigations using NMR, SEM and image analyses. *Mar. Pet. Geol.* **2019**, *99*, 416–428. [CrossRef]

20. Li, X.; Wang, Y.; Lin, W.; Ma, L.; Liu, D.; Liu, J.; Zhang, Y. Micro-pore structure and fractal characteristics of deep shale from Wufeng Formation to Longmaxi Formation in Jingmen exploration area, Hubei Province, China. *J. Nat. Gas Geosci.* **2022**, *7*, 121–132. [CrossRef]

21. Tian, X.; Duan, X.; Sun, M.; Mohammadian, E.; Hu, Q.; Ostadhassan, M.; Liu, B.; Ke, Y.; Pan, Z. Evolution of fractal characteristics in shales with increasing thermal maturity: Evidence from neutron scattering, N2 physisorption, and FE-SEM imaging. *Energy* **2024**, *298*, 131342. [CrossRef]

22. Chang, J.; Fan, X.; Jiang, Z.; Wang, X.; Chen, L.; Li, J.; Zhu, L.; Wan, C.; Chen, Z. Differential impact of clay minerals and organic matter on pore structure and its fractal characteristics of marine and continental shales in China. *Appl. Clay Sci.* **2022**, *216*, 106334. [CrossRef]

23. Peng, N.; He, S.; Hu, Q.; Zhang, B.; He, X.; Zhai, G.; He, C.; Yang, R. Organic nanopore structure and fractal characteristics of Wufeng and lower member of Longmaxi shales in southeastern Sichuan, China. *Mar. Pet. Geol.* **2019**, *103*, 456–472. [CrossRef]

24. Li, Y.; Wang, Z.; Pan, Z.; Niu, X.; Yu, Y.; Meng, S. Pore structure and its fractal dimensions of transitional shale: A cross-section from east margin of the Ordos Basin, China. *Fuel* **2019**, *241*, 417–431. [CrossRef]

25. Hill, D.G.; Nelson, C.R. Gas productive fractured shales: An overview and update. *Gas Tips* **2000**, *6*, 4–13.

26. Zhang, J.; Li, X.; Zhang, X.; Zhang, M.; Cong, G.; Zhang, G.; Wang, F. Geochemical and geological characterization of marine–continental transitional shales from Longtan Formation in Yangtze area, South China. *Mar. Pet. Geol.* **2018**, *96*, 1–15. [CrossRef]

27. Mei, Q.; Guo, R.; Zhou, X.; Cheng, G.; Li, S.; Bai, Y.; Liu, J.; Wu, W.; Zhao, J. Pore structure characteristics and impact factors of laminated shale oil reservoir in Chang 73 sub-member of Ordos Basin, China. *J. Nat. Gas Geosci.* **2023**, *8*, 227–243. [CrossRef]

28. Cao, H.; Shi, J.; Zhan, Z.-W.; Wu, H.; Wang, X.; Cheng, X.; Li, H.; Zou, Y.-R.; Peng, P. Shale oil potential and mobility in low-to medium-maturity lacustrine shales: A case study of the Yanchang Formation shale in southeast Ordos Basin, China. *Int. J. Coal Geol.* **2024**, *282*, 104421. [CrossRef]

29. Ji, L.M.; Yan, K.; Meng, F.W.; Zhao, M. The oleaginous Botryococcus from the Triassic Yanchang Formation in Ordos Basin, Northwestern China: Morphology and its paleoenvironmental significance. *J. Asian Earth Sci.* **2010**, *38*, 175–185. [CrossRef]

30. Yang, H.; Niu, X.; Xu, L.; Feng, S.; You, Y.; Liang, X.; Wang, F.; Zhang, D. Exploration potential of shale oil in Chang7 member, upper Triassic Yanchang formation, Ordos Basin, NW China. *Pet. Explor. Dev.* **2016**, *43*, 560–569. [CrossRef]

31. Li, Y.; Gao, X.; Meng, S.; Wu, P.; Niu, X.; Qiao, P.; Elsworth, D. Diagenetic sequences of continuously deposited tight sandstones in various environments: A case study from upper Paleozoic sandstones in the Linxing area, eastern Ordos basin, China. *AAPG Bull.* **2019**, *103*, 2757–2783. [CrossRef]

32. Yang, C.; Feng, Y.; Bai, L.Q. Pore-fracture features of the marine-continental transition shales from Taiyuan Formation in northern Ordos Basin and petroleum geological implication. *Geol. Resour.* **2018**, *27*, 389–395.

33. Zhang, Z.; Lv, D.; Hower, J.C.; Wang, L.; Shen, Y.; Zhang, A.; Xu, J.; Gao, J. Geochronology, mineralogy, and geochemistry of tonsteins from the Pennsylvanian Taiyuan Formation of the Jungar Coalfield, Ordos Basin, North China. *Int. J. Coal Geol.* **2023**, *267*, 104183. [CrossRef]

34. Wang, Z.; Liu, L.; Hu, J.; Wang, F.; Li, D.; Zhang, J.; Zhu, S.; Zhang, R.; Zhao, F.; Zhang, C.; et al. Dispersion of sandy sediments during marine–continental transition: An integrated study from the Late Paleozoic western Ordos Basin. *Mar. Pet. Geol.* **2024**, *160*, 106620. [CrossRef]

35. *GB/T 19145-2022*; Determination for Total Organic Carbon in Sedimentary Rock. Standardization Administration of China: Beijing, China, 2022.

36. Industry Standards of the People's Republic of China. X-ray Diffraction Analysis Method for Clay Minerals and Common Non Clay Minerals in Sedimentary Rocks: SY/T 5163-2018. Available online: https://std.samr.gov.cn/hb/search/stdHBDetailed?id=8B1827F256BDBB19E05397BE0A0AB44A (accessed on 1 March 2019).

37. *GB/T 19144-2010*; Isolation Method for Kerogen from Sedimentary Rock. Standardization Administration of China: Beijing, China, 2010.

38. Brunauer, S.; Emmett, P.H.; Teller, E. Adsorption of gases in multimolecular layers. *J. Am. Chem. Soc.* **1938**, *60*, 309–319. [CrossRef]

39. Barrett, E.P.; Joyner, L.G.; Halenda, P.P. The determination of pore volume and area distributions in porous substances. I. Computations from nitrogen isotherms. *J. Am. Chem. Soc.* **1951**, *73*, 373–380. [CrossRef]

40. Frenkel, J. Kinetic theory of liquids. In *International Series of Monographs on Physics*; Clarendon Press: Oxford, UK, 1946.

41. Halsey, G. Physical adsorption on non-uniform surfaces. *J. Chem. Phys.* **1948**, *16*, 931–937. [CrossRef]

42. Hill, T.L. Theory of physical adsorption. In *Advances in Catalysis*; Academic Press: Cambridge, MA, USA, 1952; Volume 4, pp. 211–258.

43. Yao, Y.; Liu, D.; Tang, D.; Tang, S.; Huang, W. Fractal characterization of adsorption-pores of coals from North China: An investigation on CH4 adsorption capacity of coals. *Int. J. Coal Geol.* **2008**, *73*, 27–42. [CrossRef]

44. Thommes, M.; Kaneko, K.; Neimark, A.V.; Olivier, J.P.; Rodriguez-Reinoso, F.; Rouquerol, J.; Sing, K.S.W. Physisorption of gases, with special reference to the evaluation of surface area and pore size distribution (IUPAC Technical Report). *Pure Appl. Chem.* **2015**, *87*, 1051–1069. [CrossRef]

45. Xie, W.D.; Wang, M.; Wang, X.Q.; Wang, Y.D.; Hu, C.Q. Nano-pore structure and fractal characteristics of shale gas reservoirs: A case study of Longmaxi Formation in southeastern Chongqing, China. *J. Nanosci. Nanotechnol.* **2021**, *21*, 343–353. [CrossRef]

46. Li, X.; Jiang, Z.; Jiang, S.; Li, Z.; Song, Y.; Jiang, H.; Qiu, H.; Cao, X.; Miao, Y. Various controlling factors of matrix-related pores from differing depositional shales of the Yangtze Block in south China: Insight from organic matter isolation and fractal analysis. *Mar. Pet. Geol.* **2020**, *111*, 720–734. [CrossRef]

47. Lu, C.; Xiao, X.; Gai, H.; Feng, Y.; Li, G.; Meng, G.; Gao, P. Nanopore structure characteristics and evolution of type III kerogen in marine-continental transitional shales from the Qinshui basin, northern China. *Geoenergy Sci. Eng.* **2023**, *221*, 211413. [CrossRef]

48. Liu, B.; Mohammadi, M.-R.; Ma, Z.; Bai, L.; Wang, L.; Xu, Y.; Hemmati-Sarapardeh, A.; Ostadhassan, M. Pore structure characterization of solvent extracted shale containing kerogen type III during artificial maturation: Experiments and tree-based machine learning modeling. *Energy* **2023**, *283*, 128885. [CrossRef]

49. He, H.; Liu, P.; Xu, L.; Hao, S.; Qiu, X.; Shan, C.; Zhou, Y. Pore structure representations based on nitrogen adsorption experiments and an FHH fractal model: Case study of the block Z shales in the Ordos Basin, China. *J. Pet. Sci. Eng.* **2021**, *203*, 108661. [CrossRef]

50. Liu, K.; Ostadhassan, M.; Jang, H.W.; Zakharova, N.V.; Shokouhimehr, M. Comparison of fractal dimensions from nitrogen adsorption data in shale via different models. *RSC Adv.* **2021**, *11*, 2298–2306. [CrossRef] [PubMed]

51. Wang, X.; Zhu, Y.; Wang, Y. Fractal characteristics of micro-and mesopores in the Longmaxi Shale. *Energies* **2020**, *13*, 1349. [CrossRef]

52. Xie, W.D.; Wang, M.; Wang, H.; Duan, H.Y. Multi-scale fractal characteristics of pores in transitional shale gas reservoir. *Nat. Gas Geosci.* **2022**, *33*, 451–460.

53. Liu, R.B.; Wei, Z.H.; Jia, A.Q.; He, S.; Hou, Y.G.; He, Q.; Wang, T.; Zeng, Y.; Yang, R. Fractal characteristics of pore structure in deep overpressured organic-rich shales in Wufeng-Longmaxi formation in southeastern Sichuan and its geological significance. *Earth Sci.* **2023**, *48*, 1496–1516.

54. Loucks, R.G.; Reed, R.M.; Ruppel, S.C.; Jarvie, D.M. Morphology, genesis, and distribution of nanometer-scale pores in siliceous mudstones of the Mississippian Barnett Shale. *J. Sediment. Res.* **2009**, *79*, 848–861. [CrossRef]

55. Klaver, J.; Hemes, S.; Houben, M.; Desbois, G.; Radi, Z.; Urai, J.L. The connectivity of pore space in mudstones: Insights from high-pressure Wood's metal injection, BIB-SEM imaging, and mercury intrusion porosimetry. *Geofluids* **2015**, *15*, 577–591. [CrossRef]

56. Zhang, J.; Tang, Y.; He, D.; Sun, P.; Zou, X. Full-scale nanopore system and fractal characteristics of clay-rich lacustrine shale combining FE-SEM, nano-CT, gas adsorption and mercury intrusion porosimetry. *Appl. Clay Sci.* **2020**, *196*, 105758. [CrossRef]

57. Zhao, L.Y.; Wu, Z.L.; Zhong, Y.; Xia, P.; Wei, Y.L.; Liu, J.G.; Wang, K.; Chen, S.W. Pore characteristic and its influencing factors of Longtan shale in Dahebian syncline, Liupanshui coalfield, western Guizhou. *Nat. Gas Geosci.* **2024**, *35*, 1236–1248.

58. Li, A.; Ding, W.; He, J.; Dai, P.; Yin, S.; Xie, F. Investigation of pore structure and fractal characteristics of organic-rich shale reservoirs: A case study of Lower Cambrian Qiongzhusi formation in Malong block of eastern Yunnan Province, South China. *Mar. Pet. Geol.* **2016**, *70*, 46–57. [CrossRef]

59. Yang, C.; Zhang, J.; Wang, X.; Tang, X.; Chen, Y.; Jiang, L.; Gong, X. Nanoscale pore structure and fractal characteristics of a marine-continental transitional shale: A case study from the lower Permian Shanxi Shale in the southeastern Ordos Basin, China. *Mar. Pet. Geol.* **2017**, *88*, 54–68. [CrossRef]

60. Shao, X.; Pang, X.; Li, Q.; Wang, P.; Chen, D.; Shen, W.; Zhao, Z. Pore structure and fractal characteristics of organic-rich shales: A case study of the lower Silurian Longmaxi shales in the Sichuan Basin, SW China. *Mar. Pet. Geol.* **2017**, *80*, 192–202. [CrossRef]

61. Yang, R.; He, S.; Yi, J.; Hu, Q. Nano-scale pore structure and fractal dimension of organic-rich Wufeng-Longmaxi shale from Jiaoshiba area, Sichuan Basin: Investigations using FE-SEM, gas adsorption and helium pycnometry. *Mar. Pet. Geol.* **2016**, *70*, 27–45. [CrossRef]

62. Cao, T.; Song, Z.; Wang, S.; Xia, J. Characterization of pore structure and fractal dimension of Paleozoic shales from the northeastern Sichuan Basin, China. *J. Nat. Gas Sci. Eng.* **2016**, *35*, 882–895. [CrossRef]

63. Sakhaee-Pour, A.; Li, W. Fractal dimensions of shale. *J. Nat. Gas Sci. Eng.* **2016**, *30*, 578–582. [CrossRef]

64. Wang, F.; Zai, Y. Fractal and multifractal characteristics of shale nanopores. *Results Phys.* **2021**, *25*, 104277. [CrossRef]

65. Xiao, L.; Li, Z.; Yang, Y.D.; Tang, L.; Liang, Z.K.; Yu, H.L.; Hou, Y.F.; Wang, L.W. Pore structure and fractal characteristics of different lithofacies shales of the Lower Silurian Longmaxi formation of in Southeast Chongqing. *Sci. Tech. End Eng.* **2021**, *21*, 512–521.

66. Li, F.; Dang, W.; Wang, F.; Nie, H.; Feng, Y.; Liu, Q.; Sun, J.; Ma, Y. Insights into the Process of Gas Release from Organic-Rich Shale: Release Characteristics and Controlling Factors. *Geofluids* **2023**, *2023*, 8102826. [CrossRef]

67. Li, X.; Chen, S.; Wu, J.; Zhang, J.; Zhao, S.; Xia, Z.; Wang, Y.; Zhang, S.; Zhang, J. Microscopic occurrence and movability mechanism of pore water in deep shale gas reservoirs: A typical case study of the Wufeng-Longmaxi Formation, Luzhou block, Sichuan Basin. *Mar. Pet. Geol.* **2023**, *151*, 106205. [CrossRef]

68. Shi, W.; Zhu, L.; Guo, M.; Huang, Z.; Wang, G.; Lin, L.; He, L.; Liao, Y.; He, H.; Gong, J. Assessment of CO_2 fracturing in China's shale oil reservoir: Fracturing effectiveness and carbon storage potential. *Resour. Conserv. Recycl.* **2023**, *197*, 107101. [CrossRef]

69. Zang, Y.; Wang, H.; Wang, B.; Ni, J.; Wang, T.; Zhang, W.; Zhang, Y.; Tian, S. Fracture propagation morphology and parameter optimization design of pre-CO_2 hybrid fracturing in shale oil reservoirs, Ordos Basin. *Geoenergy Sci. Eng.* **2024**, *238*, 212849. [CrossRef]